

# Enhanced ionization in small rare gas clusters

Christian Siedschlag and Jan M. Rost  
Max-Planck-Institute for the Physics of Complex Systems,  
Nöthnitzer Str. 38, D-01187 Dresden, Germany  
(Dated: October 28, 2018)

A detailed theoretical investigation of rare gas atom clusters under intense short laser pulses reveals that the mechanism of energy absorption is akin to *enhanced ionization* first discovered for diatomic molecules. The phenomenon is robust under changes of the atomic element (neon, argon, krypton, xenon), the number of atoms in the cluster (16 to 30 atoms have been studied) and the fluency of the laser pulse. In contrast to molecules it does not disappear for circular polarization. We develop an analytical model relating the pulse length for maximum ionization to characteristic parameters of the cluster.

## I. INTRODUCTION

Building the bridge between atomic and solid state physics, cluster physics has become a vivid research field of its own. While the static properties of clusters are by now well understood, there remain many open problems concerning the dynamics of clusters under external perturbations. In the case of weak perturbations, linear response theory has proven to be a valid tool for the investigation of dynamical properties [1]; but with increasing strength of the perturbation the description of the cluster evolution becomes more and more involved [2].

On the other hand, experimental studies of (mostly) rare gas cluster interaction with highly charged projectiles as well as with short, intense laser pulses have produced a number of interesting results calling for an explanation. Experiments exploring the interaction of rare gas clusters with intense laser light have shown a big increase of energy absorption compared to the single atom case [3, 4, 5, 6, 7, 8]. When irradiated with a  $10^{15}\text{W}/\text{cm}^2$  femtosecond laser whose wavelength is in the optical regime, one observes, depending on the cluster size and the atomic element, ionic charge states of up to 40. These high charge states let the fragmenting ions gain an enormous amount of kinetic energy. The most spectacular example for this highly energetic process has certainly been the recent experimental observation of nuclear fusion in a cluster [9].

Here, we focus on clusters of some 10 atoms. We have developed a model containing the essential features of the interaction between the cluster and the laser field. It will be shown that energy absorption from the laser pulse proceeds through a mechanism originally discovered for diatomic molecules (*enhanced ionization* (ENIO) [10, 11]), whose generalization for the case of small clusters will be presented.

The paper is organized as follows: after introducing the numerical model and comparing it to other types of simulations already existing in the literature in section II, we investigate the dependence of energy absorption and ionization yield on the pulse length in a series of clusters in section III. From the results of these calculations a generic behavior emerges which can be explained by in-

volving the above-mentioned enhanced ionization mechanism as explained in section IV. We give strong evidence that this mechanism should play an important role in the laser-cluster interaction over a large range of parameters detailed in section V. Finally we condense our picture of the ionization process into a simple analytical expression which quantifies the role of the experimentally accessible variables like cluster size or atomic element on the process of energy absorption in section VI. The last section VII summarizes our work. Atomic units are used if not stated otherwise.

## II. THE CLUSTER MODEL

### A. Theoretical formulation and numerical implementation

Since the dimension of the problem is far too high to allow for an exact quantum mechanical treatment we have formulated a model to describe the dynamics of rare gas clusters in strong laser fields. We resort to a classical treatment, with a few but essential quantum mechanical elements.

Initially, before the onset of the laser pulse, we find the equilibrium ground state configuration of the cluster with Lennard-Jones interaction between the neutral cluster atoms. The global minima for this potential are readily available. The electrons are assumed to be localized at the nuclei.

After fixing the initial shape of the cluster, we start the time evolution switching on the laser pulse [12]. For the electrons, this evolution consists of two parts: firstly, the modeling of the bound state and the process of ionization from this state; secondly, the propagation after being ionized from an atom. We will refer to the first process as *inner ionization*, in contrast to the *outer ionization*, which has the effect that an electron leaves the cluster. Inner ionization contains processes beyond classical mechanics, while the subsequent propagation and (eventually) outer ionization is described classically via integration of Newton's equations.

When irradiating a cluster with intense laser light, two processes can lead, at least in principle, to inner ioniza-

tion: *field ionization* and *electron impact ionization*. In the case of field ionization, the electric field inside the cluster (initially only the laser field, later the combined field of laser, ions and electrons) leads to a lowering of the potential barriers, so that an electron can leave its mother atom via tunneling [13] or even *over-the-barrier* [14]. Electrons which are already inner ionized, but not yet outer ionized, can further lead to electron impact ionization. This mechanism was shown to play almost no role in small clusters [15], as the average free path length with respect to electron impact ionization is much larger than the cluster radius. For this reason we only consider field ionization in our model.

The model is implemented as follows. Before the onset of the pulse, the electrons of the cluster are assumed to be localized at the atomic positions; the bare nucleus and all the electrons of an atom are treated as one neutral classical particle. It is only later that the electrons (through inner ionization) are born as separate classical particles. Hence, the number of particles in our simulation changes with time.

Two classical charged particles at positions  $\vec{r}_1$  and  $\vec{r}_2$  interact via the potential

$$V(\vec{r}_1, \vec{r}_2) = Z_1 Z_2 \left( |\vec{r}_1 - \vec{r}_2|^2 + a_{Z_1} + a_{Z_2} \right)^{-1/2}, \quad (1)$$

where  $Z_1$  and  $Z_2$  are the charges of the two particles. The  $a_{Z_i}$  are softcore parameters, which help to regularize the Coulomb singularity. We are using a  $Z$ -dependent  $a$ , so that the depth of the atomic potential can be adjusted to the current binding energy. To determine  $a_Z$ , we proceed as follows:

- For electrons,  $a$  has been chosen to be 0.1, i.e.  $a_{-1} = 0.1$
- For an electron which is localized in the minimum of the potential of an atom with charge  $Z$ , we demand

$$\frac{-Z}{\sqrt{a_Z + a_{-1}}} = E_{\text{bind}}(Z) + \epsilon \quad (2)$$

with a small positive parameter  $\epsilon = 0.01$ . Then we can solve for  $a_Z$

$$a_Z = \frac{Z^2}{E_{\text{bind}}^2 + 2\epsilon E_{\text{bind}} + \epsilon^2} - a_{-1}. \quad (3)$$

At every time step  $dt$ , we calculate for each atom the ionization probability of the outermost electron in the following fashion: if  $\vec{B}_j$  is the total electric field at the position  $\vec{R}_j$  of atom  $j$ ,

$$\vec{B}_j = \vec{\nabla}_{R_j} \left[ \sum_{i \neq j} \frac{Z_i}{\sqrt{(\vec{R}_j - \vec{R}_i)^2 + a_{Z_i} + 0.1}} \right] + \vec{\epsilon}_p f(t), \quad (4)$$

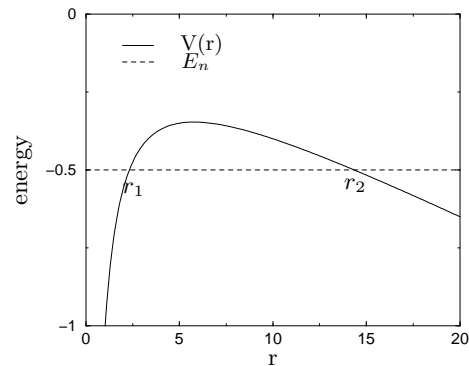


FIG. 1: Tunneling from a bound state with energy  $E_n$  in the potential  $V(r)$

with the polarization vector  $\vec{\epsilon}_p$  of the laser field, we calculate the tunneling integral in the direction of  $\vec{B}$ :

$$I(t) = \exp \left[ -2 \int_{r_1}^{r_2} \sqrt{2(V(r) - E_n)} dr \right]. \quad (5)$$

The role of  $r_1$  and  $r_2$  is shown in Fig. 1 where  $V(r)$  contains the Coulombic potential terms and those coming from the laser field. The energy level  $E_n$  is defined as

$$E_n := E_n^{\text{Atom}} + V(0) - \frac{Z_{\text{Atom}} + 1}{\sqrt{a_{Z_{\text{Atom}}} + 0.1}}. \quad (6)$$

Hence, the atomic energy level is shifted by the surrounding charges and the laser potential; the potential of the atom from which the electron will be ionized has to be subtracted because its influence is already contained in  $E_n^{\text{Atom}}$ . The positions  $r_1$  and  $r_2$ , where  $E_n$  crosses the potential curve  $V(r)$ , are determined numerically; the search for  $r_2$  is continued until  $I(t) < 10^{-10}$ . If we find a position  $r'$  along the direction of  $\vec{B}$  with  $dV/dr|_{r=r'} = 0$  and  $E_n > V(r)$  for  $r \leq r'$ , over-the-barrier ionization is possible. In this case we simply put  $I(t) = 1$ . The tunneling rate  $w(t)$  is then the tunneling probability  $I(t)$  multiplied with the frequency of the electron hitting the potential barrier. In a semiclassical picture, this frequency is just the inverse of the Kepler period  $T_n$  belonging to an orbit with binding energy  $E_n$ :

$$T_n = \pi(Z_{\text{Atom}} + 1)/(2E_n^3)^{-1/2}. \quad (7)$$

Hence, the tunneling rate is

$$w(t) = I(t)/T_n. \quad (8)$$

The tunneling probability over a unit of time  $dt$  is  $P(t) = w(t) dt$ . By comparison with a random number  $z$  (is  $P(t) > z$ ?) we decide if the electron in question tunnels. If so, we place the electron, which now becomes a classical particle, outside the potential barrier as close to  $r_2$  as possible, with the exact position and momentum of the electron determined by conservation of the total

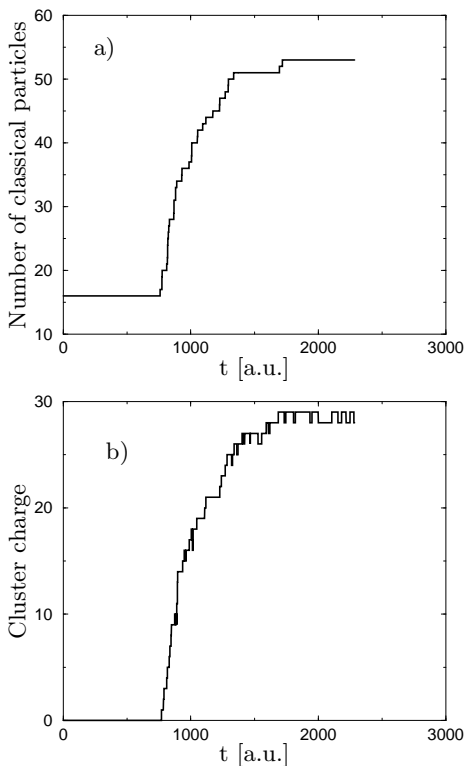


FIG. 2: Number of classically treated particles (a) and total charge of the cluster (b).

energy [16]. If the ionization happens to be over-the-barrier, we put the electron on top of the barrier, where  $dV/dr = 0$ . The atomic charge is raised by 1 and the next virtual electron is allowed to tunnel.

The particles are classically propagated by integrating Newton's equations of motion. We have used a symplectic integrator [17] with a time step of  $dt = 0.1$ .

### B. A typical run

Although later we will use a Monte Carlo ensemble to calculate experimentally accessible observables, for a qualitative understanding of the phenomena it is sufficient to have a closer look on a single event, since the overall behavior of the ensemble members is quite similar. As an example we consider a  $\text{Ne}_{16}$ -cluster. The applied pulse has a peak intensity of  $I = 10^{15} \text{ W/cm}^2$ , a frequency of  $\omega = 0.055 \text{ a.u.}$  (780 nm) and it extends over 20 cycles, so that the pulse length is approx.  $T \approx 55 \text{ fs}$ . We chose a  $\sin^2$ -function for the pulse envelope, i.e. the pulse is of the form

$$f(t) = F \sin^2(\pi t/T) \sin(\omega t) \quad (0 \leq t \leq T). \quad (9)$$

Fig. 2 shows the total number of classically treated particles and the cluster charge, i.e. the number of electrons

which have left the cluster, as a function of time. After approximately 750 fs the intensity of the laser is sufficiently high for the first inner ionization event, followed by a rapid increase of the number of classical particles as well as the cluster charge. Obviously, the ionization of the first few electrons leads to an 'avalanche effect': the inner ionized electrons create a strong electric field inside the cluster, which helps to inner ionize further electrons (this is reminiscent of the *ionization ignition* mechanism [18]).

Fig. 3 shows the energy absorbed by the cluster and the mean interionic distance, again as a function of time. If  $\mathcal{K}$  is the set of nuclei with mass  $M$ ,  $\mathcal{E}$  the set of inner ionized electrons (mass  $m$ ) already treated classically and  $\mathcal{G}$  the set of electrons which are still bound, the cluster energy is defined as

$$\sum_{i \in \mathcal{K}} \frac{P_i^2}{2M} + \sum_{i \in \mathcal{E}} \frac{p_i^2}{2m} + \sum_{i,j \in \mathcal{K} \cup \mathcal{E}} V_{ij} + \sum_{i \in \mathcal{G}} E_i^{\text{bind}} \quad (10)$$

$$+ \sum_{i \in \mathcal{K}} Z_i (\vec{\epsilon}_p \cdot \vec{R}_i) f(t) - \sum_{i \in \mathcal{E}} (\vec{\epsilon}_p \cdot \vec{r}_i) f(t). \quad (11)$$

The absorbed energy is the difference of the total energies before and after the laser pulse. As we can see, this rather small cluster can already absorb a considerable amount of energy. The oscillations are due to the ponderomotive potential and have no direct influence on the net energy absorption. As the cluster gets charged, it begins to expand, i.e. the mean interionic distance will increase. For a cluster consisting of  $N$  atoms, it is defined as

$$R(t) = \left( \frac{1}{N} \sum_{i=1}^N \min_{i \neq j} \{ |\vec{R}_i - \vec{R}_j|^2 \} \right)^{1/2}. \quad (12)$$

At the intensity used here, the cluster disintegrates completely, i.e. we observe only atomic fragments after the pulse. Note that the expansion of the cluster takes place adiabatically compared to the time scales of the laser frequency and the electronic motion, but on the same time scale as the pulse length. Hence, it is possible to explore radius-dependent properties of the cluster by varying the pulse length.

### C. Comparison to other models

Similar models for the theoretical description of small rare gas clusters in strong laser fields have been proposed by other authors. The common feature is the use of classical mechanics as the basic ingredient of the description; the main differences lie in the treatment of inner ionization.

#### 1. The onion model

Following its name this model [18], as ours, treats the weakest bound electron per atom or ion as the active

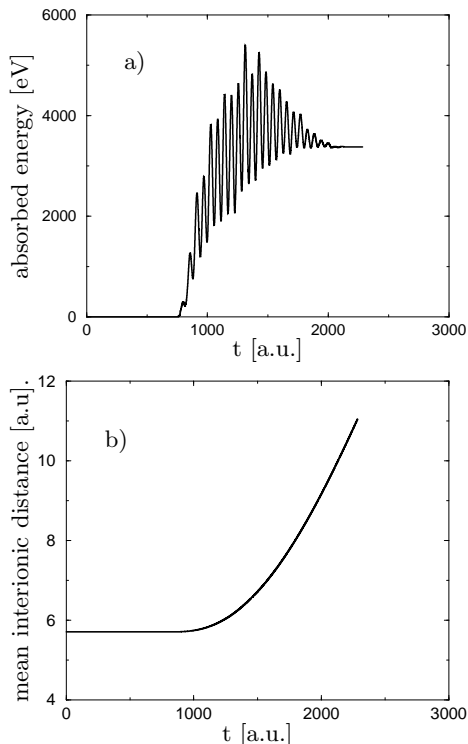


FIG. 3: Absorbed energy (a) and mean interionic distance (b) (see Eq. (12)) as a function of time.

electron which can be inner ionized. However, tunneling is not included. Instead, the active electron circles its mother ion on a Kepler orbit with an energy corresponding to the quantum mechanical binding energy. This orbit is then deformed in time by the laser field and the surrounding charges, and inner ionization can take place, which is defined by reaching a certain distance  $r_c$  from the mother ion. If the electron exceeds this distance, it is assumed to be inner ionized, and the next electron is put onto a (now deeper bound) Kepler orbit.

In common with our model, inner ionization takes place sequentially, and the already inner ionized electrons are propagated classically. By neglecting any tunneling contributions, the first inner ionization will take place a certain time  $\delta t$  later than in our case. As we will see, this delay can have a significant influence on the subsequent dynamics of the cluster rendering a fully classical treatment as in the onion model problematic.

### 2. Tunneling via the Landau rate

In this ansatz [19] the tunneling mechanism is taken into account, but the tunneling integral is not calculated explicitly. Instead, the time dependent tunneling prob-

ability is estimated using the Landau tunneling rate [20], which has been established for the case of an atom in a quasistatic laser field. For this purpose, the total electric field (laser + electrons + ions) at the position of an atom is used. For inner ionization to happen in this model the field strength has to be strong enough at just one point, namely, the position of the atom. Hence, an electron which comes by chance close to an ion will create *locally* such a strong field that ionization can hardly be avoided. In our model, in contrast, the entire environment of an atom must be suitable for ionization. Consequently, we get lower ionization rates than in [19] but in better agreement with [15].

### 3. Using the full Coulomb potential

In a third model [15], the full tunneling integral is calculated at each time step as in our case. Moreover, the authors do not use a softcore potential but employ the full Coulomb potential and regularize the singular equations of motion. The use of the full Coulomb potential may, at first glance, seem to be an advantage. However, it leads to the problem of classical autoionization: a classical electron in a Coulomb potential can be arbitrarily deeply bound, since there is no uncertainty relation. The corresponding energy gained is available as kinetic energy for the ionization of other electrons. In our model, this unphysical behavior is avoided by requiring the minimum of the softcore potential to coincide with the quantum mechanical binding energy.

In [15] a recapture mechanism was built in to account for this problem, which can transform already classically treated electrons back into a virtual bound state existence. Not to mention the peculiarities which arise when defining the exact conditions for recapture in a many-particle environment, the numerical expenditure is higher than in our case. Nevertheless, the ionization yields calculated with this model agree quite well with our results.

## III. ABSORPTION PROPERTIES FOR DIFFERENT PULSE LENGTHS

To investigate how the expansion of a cluster during the interaction with a strong laser pulse influences its absorption behavior, we have calculated the absorbed energy and the average ionic charges after the interaction for various pulse lengths. To keep the amount of energy delivered by these pulses fixed, we demand the fluency to be constant, i.e.

$$E(T) := \int_0^T f^2(t) dt = \text{const.} \quad (13)$$

For a pulse of the shape of Eq. (9), we obtain

$$E(t) = 3F^2T/16. \quad (14)$$

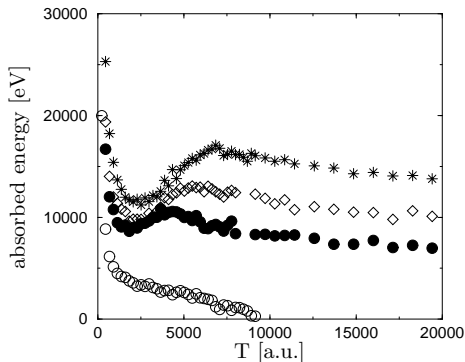


FIG. 4: Energy absorption of  $\text{Ne}_{16}$  ( $\circ$ ),  $\text{Ar}_{16}$  ( $\bullet$ ),  $\text{Kr}_{16}$  ( $\diamond$ ), and  $\text{Xe}_{16}$  ( $\star$ ) for different pulse lengths (see text).

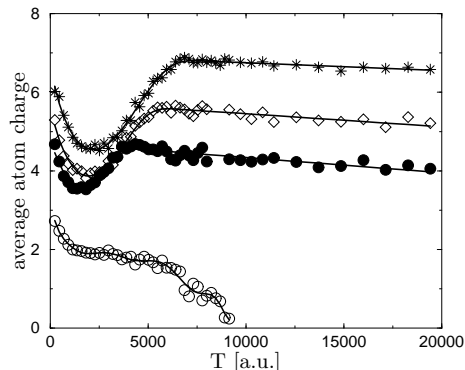


FIG. 5: Average atom charge as a function of pulse lengths for different clusters, see Fig. 4. The solid lines are to guide the eye.

For the reference pulse, we chose the parameters already used in the single run from the previous section:  $F = 0.16$  a.u.,  $\omega = 0.055$  a.u. and a pulse length of 20 cycles. Shorter pulses have a higher maximum field strength and longer pulses a lower maximum field strength, respectively. The results were obtained by averaging over a Monte Carlo ensemble consisting of 20 clusters.

### A. The light $\text{Ne}_{16}$ cluster: almost atomic behavior

The first cluster we consider is  $\text{Ne}_{16}$ . The absorbed energy and the average atomic charges as a function of pulse length under the constraint of Eq. (13) are shown in Figs. 4 and 5, respectively.

Both curves decrease monotonically with increasing pulse length. The average atomic charge exhibits a plateau for pulse lengths around  $T = 3000$  a.u.. At this point, we can already suspect that the plateau might have its origin in the expansion of the cluster during the pulse. However, in the case of  $\text{Ne}_{16}$  its effect seems to be rather small. In fact, Neon clusters of this size behave more like

atoms. This changes for heavier rare gases.

### B. Generic cluster behavior in $\text{Ar}_{16}$

The absorbed energy (Fig. 4) and average atomic charge (Fig. 5) for an  $\text{Ar}_{16}$  cluster decrease monotonically for very short pulse lengths only. Both quantities start to rise again for  $T \approx 2000$  a.u., reaching a maximum at an optimal pulse length of  $T \approx 4500$  a.u. (we will refer to this optimal pulse length as  $T^*$  subsequently) before they ultimately decrease. The average charge state reached at  $T = T^*$  is around 4.5, which is considerably higher than what one would expect from a single Argon atom.

The maximum is much more pronounced for the ionization yield than for the absorbed energy for two reasons. Firstly, for shorter pulses the mean internuclear distance just after the pulse will in general be smaller than for longer pulses, so that the Coulomb explosion energy will increase with decreasing pulse length. Secondly, the ionized electrons, which can be considered to be quasi-free, acquire a higher kinetic energy for shorter pulses, since the intensity is higher than for longer pulses. These two effects wash out the minimum in the curve for the absorbed energy and decrease the contrast between minimum and maximum.

We will postpone the further discussion and explanation of this structure after we have taken a look at the corresponding results for  $\text{Kr}_{16}$  and  $\text{Xe}_{16}$ .

### C. Same qualitative behavior as for Argon: $\text{Kr}_{16}$ and $\text{Xe}_{16}$

Qualitatively, the behavior for  $\text{Kr}_{16}$  as well as for  $\text{Xe}_{16}$  is the same as for  $\text{Ar}_{16}$ : the energy absorption and the average atomic charge peak for a certain pulse length  $T^*$ , which depends on the type of the cluster. The average atomic charge increases with the atomic mass, reaching an average of almost  $7^+$  for the  $\text{Xe}_{16}$  cluster; this is of course due to the decreasing binding energies of the electrons in the heavier elements. The value of  $T^*$  is changing for different clusters; we will come back to this point later, after we have understood the reason for the existence of  $T^*$ .

## IV. CALCULATIONS WITH FIXED NUCLEI

The existence of an optimal pulse length  $T^*$  can be related to an optimal cluster geometry with critical radius  $R^*$ , which maximizes the energy absorption (and also the ionization) of a small rare gas cluster in a strong field. Given the existence of such a critical radius, which should be larger than the equilibrium radius  $R_0$ , the occurrence of  $T^*$  can be readily explained.

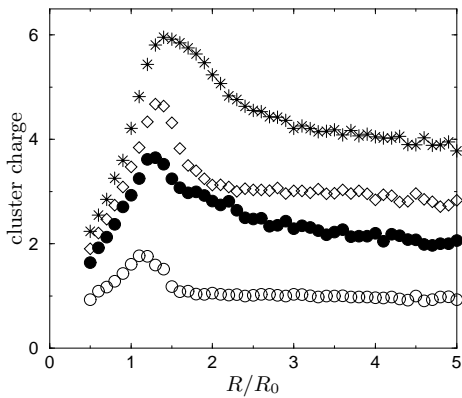


FIG. 6: Cluster charge, calculated with fixed nuclei, as a function of the mean interionic distance (see Eq. (12), in units of the equilibrium mean interionic distance  $R_0$ ) for  $\text{Ne}_{16}$  (○),  $\text{Ar}_{16}$  (●),  $\text{Kr}_{16}$  (◇) and  $\text{Xe}_{16}$  (★).

For very short pulse lengths, the cluster has almost no time to expand during the pulse, so that the critical radius will be reached only well after the pulse is already switched off. For longer and longer pulses, the cluster will reach  $R^*$  at earlier and earlier times. For a certain pulse length  $T^*$ , the time of reaching  $R^*$  will roughly coincide with the maximum of the pulse, which leads to optimal absorption. If the pulses are becoming even longer,  $R^*$  will be reached already before the maximum of the pulse *and* the maximum intensity is decreasing due to the energy normalization (Eq. (13)). Both effects lead to a decrease in energy absorption as well as in the average atomic ionization for  $T > T^*$ .

What remains to be shown is that the critical radius  $R^*$  really exists and to explain its origin. To this end, we have calculated the cluster ionization yield for *different*, but *fixed* cluster radii. We have accomplished this by applying a scaling transformation

$$\vec{R}_i^0 \Rightarrow \lambda \vec{R}_i^0 \quad (15)$$

to the atomic positions, with  $\lambda = 1$  corresponding to the ground state configuration. The pulse we use is the reference pulse for the calculations of the last section, i.e. of the form Eq. (9) with  $F = 0.16$  a.u.,  $\omega = 0.055$  a.u. and 20 cycles length. The results of these calculations are shown in Fig. 6. For all four clusters under consideration, we observe the existence of a critical radius  $R^*$  [21], which is larger than the equilibrium one. This means that it will be reached during the expansion the clusters undergo when irradiated with intense laser light. The results of the previous section thus can indeed be explained by the existence of  $R^*$ . The question remaining to be settled is: which mechanism is responsible for  $R^*$ ? In principle, two possibilities are available: first, it could be a resonance effect where the electrons inside the cluster oscillate at a certain characteristic frequency which would coincide with the laser frequency at a certain cluster size. This kind of mechanism is well known from the

plasmon resonance in metal clusters [22]; being originally a weak-field-concept, the plasmon has been claimed to play an important role also in the strong field regime [3]. However, one needs a delocalized electron cloud to create a plasmon resonance; in rare gas clusters, this condition is not fulfilled.

The second mechanism would be a generalization of a concept first discovered for linear, diatomic molecules [10, 11, 23], called *enhanced ionization* (ENIO). It can be qualitatively explained by looking at the potential curve of such a molecule exposed to a quasistatic electric field (see Fig. 7): the upper energy level of the two levels  $1\sigma_+$  and  $1\sigma_-$ , which emanate from the bonding and the antibonding molecular orbital when an electric field is switched on, will lie above the inner potential barrier but below the outer potential barrier when the internuclear distance  $R$  is rather small. On the other hand, when  $R$  is rather large, the level will lie below the inner barrier but above the outer barrier (using the terms introduced in the previous section, we can say that *inner ionization* is easier than *outer ionization* for small  $R$  and vice versa for large  $R$ ). For an intermediate value of  $R$ , typically around 6-8 a.u., the interplay between inner and outer ionization will lead to a maximum in the ionization rate.

This mechanism has been shown to be operative not only in linear molecules, but also in triatomic molecules of triangular shape [24, 25]. In this case, the simple picture of Fig. 7 is already slightly distorted, and it is more appropriate to think of enhanced ionization in terms of an optimal balance between inner and outer ionization, which makes the generalization of the mechanism to a true many-body system like a cluster much easier.

One characteristic feature of the enhanced ionization mechanism is its relative insensitivity on the frequency of the applied laser field. As long as the quasistatic picture is valid, the value of  $R^*$  should not change significantly with the laser frequency. On the other hand, any resonance-type mechanism like the plasmon picture should exhibit a strong dependence of  $R^*$  on the laser frequency. We have calculated the ionization yield of  $\text{Ne}_{16}$  and  $\text{Ar}_{16}$  for three different frequencies, with the results shown in Fig. 8. The position of  $R^*$  does hardly change for different laser frequencies. Hence, we can exclude any kind of resonance behavior in favor of the enhanced ionization mechanism.

Although the position of  $R^*$  does not change with the laser frequency, the ionization yield does. This is due to the fact that electrons which are already outer ionized tend to leave the cluster region faster when the frequency is smaller: the quiver amplitude of an electron in an electric field of frequency  $\omega$  is proportional to  $1/\omega^2$ . Hence, on average in fields of higher frequencies the already ionized electrons will stay closer to the cluster for a longer time and lead to an increased field ionization rate.

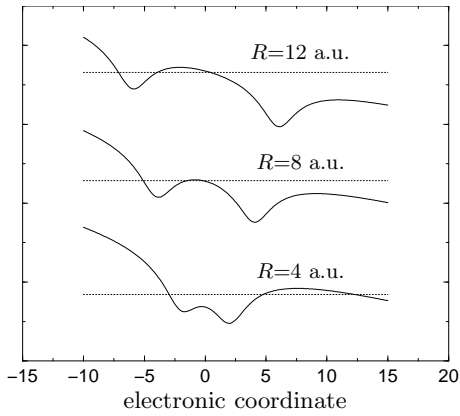


FIG. 7: Schematic potential curves and the upper energy level  $1\sigma_+$  of a diatomic molecule for different internuclear distances.

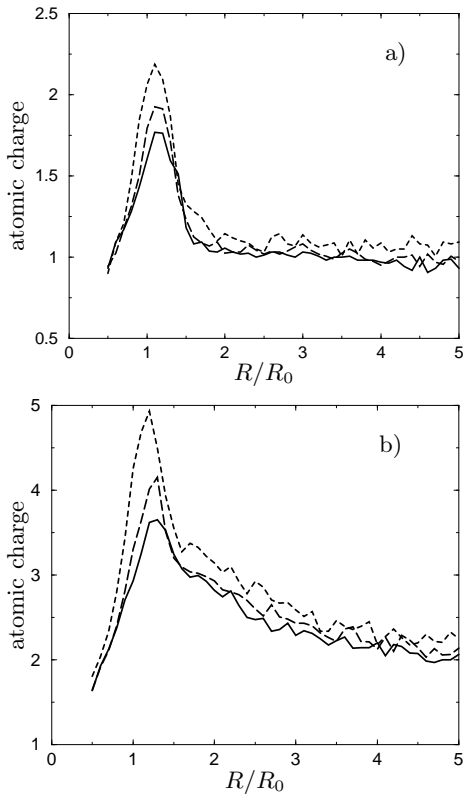


FIG. 8: Atomic ionization yield for the three frequencies  $\omega = 0.055$  a.u. (solid line),  $\omega = 0.075$  a.u. (long dashed line) and  $\omega = 0.11$  a.u. (dashed line) for  $\text{Ne}_{16}$  (a) and  $\text{Ar}_{16}$  (b). The pulse length was  $T = 55$  fs.

## V. EXPLORATION OF THE PARAMETERS CONTROLLING LASER-CLUSTER INTERACTION

Having established the basic mechanism for coupling energy from the laser pulse into small rare gas clusters,

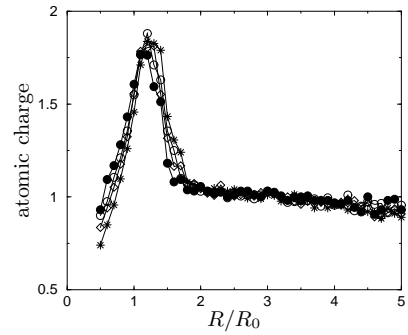


FIG. 9: Average atomic charge state as a function of the mean interionic distance for  $\text{Ne}_{16}$  (●),  $\text{Ne}_{20}$  (○),  $\text{Ne}_{25}$  (◇) and  $\text{Ne}_{30}$  (★).

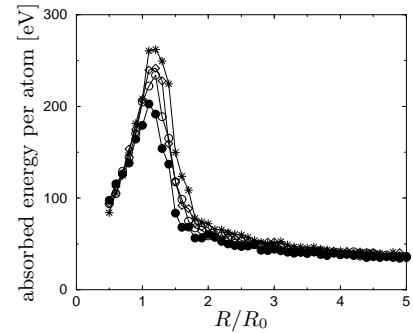


FIG. 10: Absorbed energy/atom as a function of the mean interionic distance for  $\text{Ne}_{16}$  (●),  $\text{Ne}_{20}$  (○),  $\text{Ne}_{25}$  (◇) and  $\text{Ne}_{30}$  (★).

we will explore now the influence of different parameters on this mechanism, such as cluster size, energy content of the laser pulse and laser polarization.

### A. Different cluster sizes

As in the previous section, we present the cluster response with fixed nuclei first and relate the results of these calculations to the absorption behavior when the nuclei are allowed to move. The average atomic charge and the absorbed energy were calculated as a function of the mean interionic distance again, analogous to section IV. The equilibrium value  $R_0$  does hardly change when going to bigger clusters. The variation of  $R_0$  for  $\text{Ne}_{16}$ ,  $\text{Ne}_{20}$ ,  $\text{Ne}_{25}$  and  $\text{Ne}_{30}$  is only about 0.01 a.u.. We have used the same pulse as in section IV. As can be seen from Fig. 9 and Fig. 10, the bigger clusters show almost no difference compared to  $\text{Ne}_{16}$  when the observables are normalized on the number of cluster atoms. In particular the existence of a critical distance  $R^* > R_0$  is confirmed in all cases.

There is no hint on a transition to a collective behavior at these cluster sizes. If we think of cluster physics as the

transition regime between atomic and solid state physics, we are still on the atomic side with a cluster of 30 atoms.

From the fact that the charge per atom is almost independent of the number of cluster atoms we may conclude that only the next-neighbor-atoms participate in the mechanism of enhanced ionization; otherwise the effectivity of this mechanism should change with the cluster size. The absorbed energy per atom, however, is varying with the number of atoms. This effect can be easily explained by calculating the change in the potential energy  $U(N)$  of a cluster consisting of  $N$  ions of charge  $Z$  and radius  $R$  if one adds a new ion with the same charge  $Z$  to the cluster. If one assumes that this new ion is placed at the border of the cluster, then

$$U(N+1) = U(N) + NZ^2/R. \quad (16)$$

If  $4\pi r_s^3$  denotes the volume per atom, then  $R = N^{1/3}r_s$  and

$$U(N+1) = U(N) + N^{2/3}Z^2/r_s. \quad (17)$$

With  $N$  as a continuous variable one is left with the differential equation

$$\frac{dU(N)}{dN} = \frac{N^{2/3}Z^2}{r_s}, \quad (18)$$

so that finally

$$U(N) = \frac{3}{5} \frac{N^{5/3}Z^2}{r_s}. \quad (19)$$

Hence, the potential energy per atom  $U/N$  has increases with  $N^{2/3}$  if the charge per atom is independent of  $N$ .

Proceeding from Ne to Ar clusters, one finds again that the effectivity of the ionization mechanism hardly changes when changing the cluster size, while the absorbed energy per atom increases with  $N$ , for the same reason as discussed above (see Fig. 11 and Fig. 12). However, while the Ne clusters show only a little shift of  $R^*$  as a function of cluster size, the ratio of  $R^*$  to  $R_0$  increases slightly more with increasing  $N$  for Ar. This is probably due to a larger downshift of the atomic energy levels by the increased total amount of surrounding charge when  $N$  is increased. As can be seen from Fig. 7, a downshift of the atomic energy levels leads to an increase in  $R^*$ . Since the electron release in argon clusters is larger than in neon clusters higher charged ions are generated than in neon clusters rendering this effect more pronounced for Ar clusters.

Since we have found a critical cluster radius  $R^*$  with  $R^* > R_0$  in all cases considered, it is not too surprising that we find a behavior analogous to the small clusters of Fig. 4 and Fig. 5 if the bigger clusters are allowed to expand freely. The results of these calculations, with the pulse normalization being identical to section III, are shown in Fig. 13 and Fig. 14. For clarity, we have plotted the total cluster charge instead of the average atomic charge, which is almost the same independent of  $N$ .

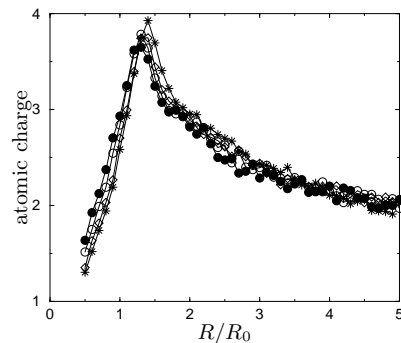


FIG. 11: Average atomic charge state as a function of the mean interionic distance for Ar<sub>16</sub> (●), Ar<sub>20</sub> (○), Ar<sub>25</sub> (◇) and Ar<sub>30</sub> (★).

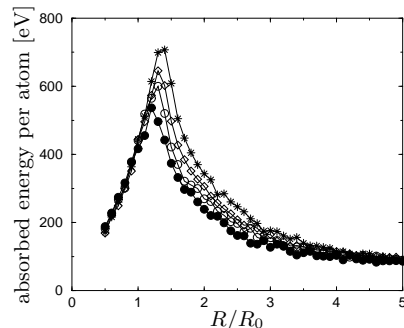


FIG. 12: Absorbed energy/atom as a function of the mean interionic distance for Ar<sub>16</sub> (●), Ar<sub>20</sub> (○), Ar<sub>25</sub> (◇) and Ar<sub>30</sub> (★).

The overall structure of the curves is seen to be quite similar throughout the different cluster sizes, as one would expect from Fig. 9 and Fig. 11. In the case of Ne clusters, the plateau which has been observed for Ne<sub>16</sub> already in Fig. 5 goes over into a small maximum with increasing  $N$ , which indicates that the enhanced ionization mechanism is slightly more efficient for larger clusters when the ions are allowed to move. One tendency which can be observed for the Ar clusters is that  $T^*$  increases with increasing  $N$ . We have seen in Fig. 11 that  $R^*$  increases also with  $N$ , so that the larger Ar clusters have to travel a longer distance until they reach the critical radius. For the Ne clusters, on the contrary, the curves show almost no shift in the  $T$ -direction when  $N$  is changed. We will investigate the dependence of the expansion process on the various cluster parameters like size and atom charge in closer detail in section VI.

## B. The influence of the pulse normalization

Changing the laser intensity  $I$  in the case of H<sub>2</sub><sup>+</sup>, with just a single electron available, leads to a decrease of  $R^*$  when  $I$  is increased and vice versa [26]. For clusters



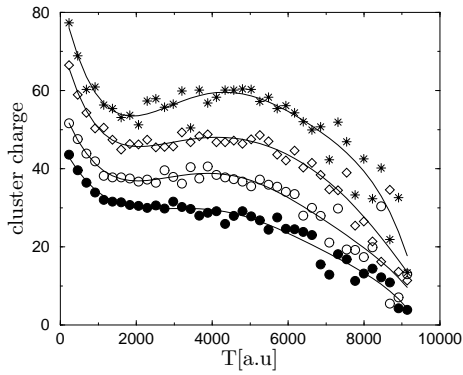


FIG. 13: Cluster charge as a function of pulse length for  $\text{Ne}_{16}$  ( $\bullet$ ),  $\text{Ne}_{20}$  ( $\circ$ ),  $\text{Ne}_{25}$  ( $\diamond$ ) and  $\text{Ne}_{30}$  ( $\star$ ). Lines are to guide the eye.

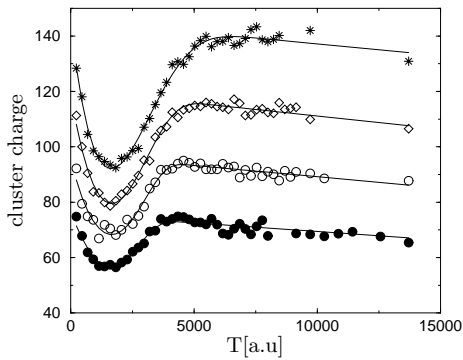


FIG. 14: Cluster charge as a function of pulse length for  $\text{Ar}_{16}$  ( $\bullet$ ),  $\text{Ar}_{20}$  ( $\circ$ ),  $\text{Ar}_{25}$  ( $\diamond$ ) and  $\text{Ar}_{30}$  ( $\star$ ). Lines are to guide the eye.

the situation is much more complicated because with increasing  $I$  lower lying energy levels will be ionized, so that it is a priori not clear in which way a change of the laser intensity (in a calculation with fixed nuclei) will influence the value of  $R^*$ . Fig. 15 shows the static ionization yields for  $\text{Ne}_{16}$ ,  $\text{Ar}_{16}$ ,  $\text{Kr}_{16}$  and  $\text{Xe}_{16}$  under the influence of the pulse used so far (i.e. a peak intensity of  $I_1 = 8.99 \cdot 10^{14} \text{W/cm}^2$ ), compared to the result of a calculation with  $I_2 = 2.19 \cdot 10^{15} \text{W/cm}^2$  (in both cases the pulse was of the form Eq. (9) with  $\omega = 0.055$  a.u. and  $T = 55$  fs). In all four cases  $R^*$  is larger than  $R_0$  and can be reached by cluster expansion. The value of  $R^*$  is, if at all, only slightly decreased in the case of higher intensity: due to the large number of electrons involved the geometry of the problem is obviously not as sensitive to the laser field strength as in the  $\text{H}_2^+$  case.

Of course, the ionization yield is higher when the intensity is increased. This leads to significantly shorter expansion times when the nuclei are allowed to move. Consequently, the optimal pulse lengths  $T^*$  are now shifted towards smaller values, as can be seen in Fig. 16 in ac-

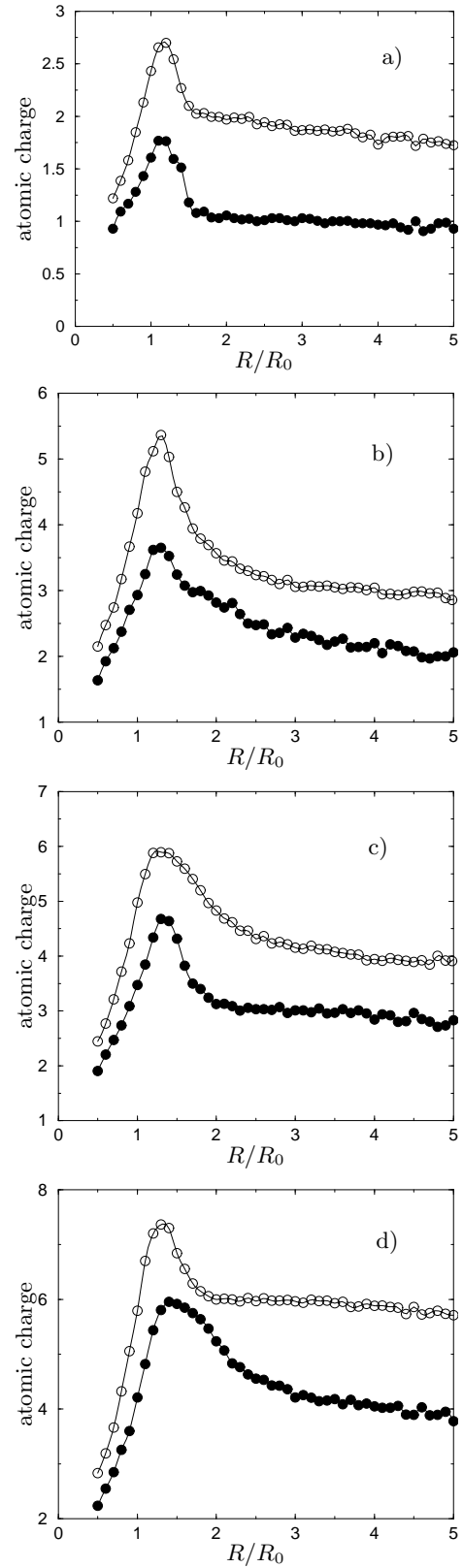


FIG. 15: Static ionization yield at the two intensities  $I_1 = 8.99 \cdot 10^{14} \text{W/cm}^2$  ( $\bullet$ ) and  $I_2 = 2.19 \cdot 10^{15} \text{W/cm}^2$  ( $\circ$ ) for  $\text{Ne}_{16}$  (a),  $\text{Ar}_{16}$  (b),  $\text{Kr}_{16}$  (c) and  $\text{Xe}_{16}$  (d). Lines are to guide the eye.

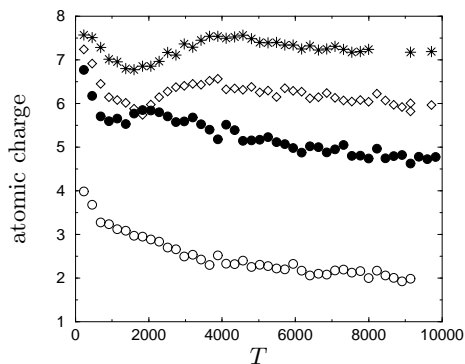


FIG. 16: Pulse length dependent ionization yields with a pulse energy corresponding to  $I_2 = 2.19 \cdot 10^{15}$  and a pulse length of 20 cycles for Ne<sub>16</sub> (○), Ar<sub>16</sub> (●), Kr<sub>16</sub> (◇) and Xe<sub>16</sub> (★).

cordance with our picture of the ionization process.

### C. Enhanced ionization and circular polarization

So far all the results presented are expected to hold also for diatomic molecules. One main difference between such a molecule and a cluster is the molecular axis: the whole picture of ENIO as sketched in Fig. 7 relies on the fact that the polarization direction of the applied laser field coincides with the internuclear axis. And indeed, experiments as well as calculations with a polarization axis perpendicular to the molecular axis have shown no signature of enhanced ionization [24, 27]. For the same reason ENIO is much less efficient under circular polarization.

On the other hand, a cluster is (in first approximation) spherically symmetric. Thus one would expect enhanced ionization to work also with circularly polarized light. To test this hypothesis, we have performed the same calculations as in the previous sections, but now with circularly polarized laser light. We have chosen the field strength of the laser such that the energy content of a pulse with a certain pulse length  $T$  remains constant when passing from linear to circular polarization: if

$$F_0 \sin^2(\pi/Tt) \sin(\omega t) \vec{e}_x \quad (20)$$

is a laser pulse with linear polarization in  $x$ -direction, then

$$F_0/\sqrt{2} \sin^2(\pi/Tt) (\sin(\omega t) \vec{e}_x + \cos(\omega t) \vec{e}_y) \quad (21)$$

is the corresponding circularly polarized pulse. With this definition the maximum field strength is decreased by a factor of  $\sqrt{2}$ . As expected, ENIO also exists for circularly polarized laser pulses. Fig. 17 shows the calculations with fixed nuclei, Fig. 18 the corresponding results with moving nuclei. In the case of static nuclei, we find that the ionization yield in the critical regime is almost as high for circular as for linear polarization (Fig. 6),

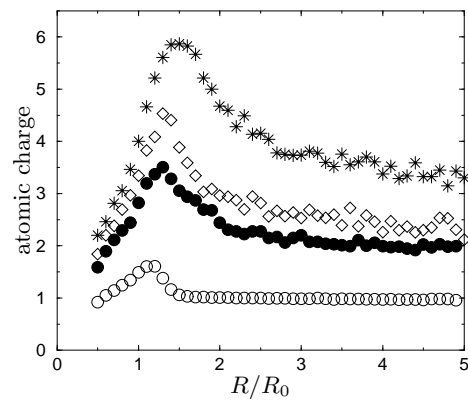


FIG. 17: Atomic charges with fixed nuclei and circular polarization for Ne<sub>16</sub> (○), Ar<sub>16</sub> (●), Kr<sub>16</sub> (◇) and Xe<sub>16</sub> (★). The pulse parameters are  $F_0 = 0.16/\sqrt{2}$  a.u.,  $\omega = 0.055$  a.u. and  $T = 55$  fs.

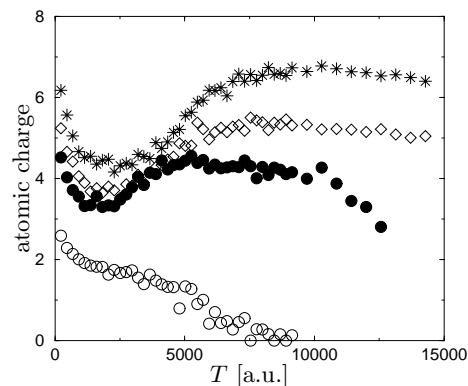


FIG. 18: Same as Fig. 17 but with moving nuclei.

in sharp contrast to the above-mentioned results for diatomic molecules. Consequently, when the nuclei are allowed to move we also get qualitatively the same results (Fig. 18) as with linear polarization (Fig. 5). It is only for rather long pulses that in the case of Ne<sub>16</sub> and Ar<sub>16</sub> the ionization yield is significantly lower than in the linear case, which is due to the reduced maximum field strength. Summarizing our exploration of different parameters we find that ENIO for clusters is a rather robust phenomenon. This has motivated us to ask if the optimum pulse length  $T^*$  can be quantitatively linked to the critical radius  $R^*$ .

## VI. ANALYTICAL FORMULA FOR THE COULOMB EXPLOSION

To isolate the relation of  $T^*$  to  $R^*$  we divide the time-dependent dynamics into three different phases: phase I denotes the time from the onset of the laser pulse until 50% of the atoms in the cluster have lost one electron due

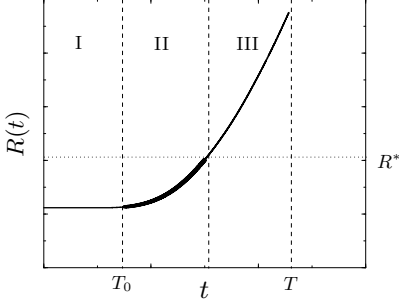


FIG. 19: Sketch of phases I, II and III during the pulse (see text)

to inner ionization. We will refer to this time as  $T_0$  subsequently. Since some of the inner ionized electrons will leave the cluster, we can say that  $T_0$  marks the beginning of the expansion process.

In this first phase inner ionization is dominated by atomic processes, the environment plays only a minor role. For a single atom/ion the time-dependent probability that the active electron is *not yet* ionized reads, in terms of the field- and binding energy dependent ionization rate  $w(f(t), E_b)$

$$P_{\text{neutral}}(t) = \exp\left(-\int_0^t w(f(t'), E_b) dt'\right), \quad (22)$$

where  $E_b$  denotes the binding energy. The probability that in a cluster consisting of  $N$  such atoms no electron has been ionized is given by

$$P_{\text{neutral}}^{\text{cluster}}(t) = [P_{\text{neutral}}(t)]^N. \quad (23)$$

The exponential dependence on  $N$  renders  $P_{\text{neutral}}^{\text{cluster}}(t)$  practically a step function. Hence, the exact value (between zero and one) for the definition of  $T_0$  is not relevant. We determine  $T_0$  from  $P_{\text{neutral}}^{\text{cluster}}(T_0) = 1/2$  which is tantamount to demanding that on average 50 % of the atoms in the cluster are singly ionized at  $T_0$ .

The second phase contains the cluster expansion up to the critical time  $T^*$ , when the critical cluster radius  $R^*$  is reached. Hence, the critical time is the sum of  $T_0$  and the expansion time  $T_{\text{exp}}$ :

$$T^* = T_0 + T_{\text{exp}}. \quad (24)$$

The third phase is finally the time from reaching  $R^*$  to the end of the pulse. A schematic picture of the different phases is shown in Fig. 19.

From  $T_0$  until the end of the pulse, the total cluster charge increases from  $Z = N/2$  to  $Z = Z_{\text{final}}$ . As a first approximation, we assume that the expansion from  $R = R_0$  to  $R = R^*$  is driven by an effective charge per atom  $\bar{Z} = \alpha Z_{\text{final}}/N$  with a constant factor  $\alpha$  which stands for the efficiency of the enhanced ionization mechanism. Furthermore, the expansion is assumed to be accomplished by the Coulomb repulsion of the nuclei only,

i.e. we neglect the influence of the laser field as well as of the electronic dynamics on the expansion process. Under these two assumptions, we can use energy conservation to write

$$\sum_{i=1}^N \frac{M}{2} v_i^2 + \sum_{(i \neq j)=1}^N \frac{\bar{Z}^2}{R_{ij}(t)} = E, \quad (25)$$

where  $R_{ij}(t) = |\vec{R}_i(t) - \vec{R}_j(t)|$ ,  $M$  is the atomic mass and  $v_i$  the respective atomic velocities. As a further approximation we assume that the expansion takes place in a homogenous and isotropic way, so that it can be described by a common expansion parameter  $\lambda(t)$  with  $\vec{R}_i(t) = \lambda(t)\vec{R}_i(0)$ . Defining

$$K_0 := \sum_{i=1}^N \frac{1}{2} M R_i^2(0)$$

$$V_0 := \sum_{(i \neq j)=1}^N \frac{(Z_{\text{final}}/N)^2}{R_{ij}(0)} \quad (26)$$

and taking into account that the kinetic energy is zero before the expansion we may write the energy balance of Eq. (25) as

$$K_0 \dot{\lambda}^2(t) + \frac{\alpha^2}{\lambda(t)} V_0 = \frac{\alpha^2}{\lambda(0)} V_0. \quad (27)$$

Finally, Eq. (27) may be rearranged as a differential equation for  $\lambda(t)$

$$\frac{d\lambda(t)}{dt} = \alpha \left[ \left(1 - \frac{1}{\lambda(t)}\right) \frac{V_0}{K_0} \right]^{1/2}, \quad (28)$$

which can be solved analytically by separation of variables for the expansion time:

$$T_{\text{exp}} = \sqrt{\frac{K_0}{V_0}} \frac{1}{\alpha} \left[ \sqrt{x(x-1)} + \log(\sqrt{x-1} + \sqrt{x}) \right]_{x=1}^{\lambda}$$

$$=: \sqrt{\frac{K_0}{V_0}} \frac{f(\lambda)}{\alpha}. \quad (29)$$

The ratio  $K_0/V_0$  determines the time scale for the expansion of the cluster. By replacing  $R_{ij}(0)$ , the distance between two ions in  $V_0$ , with the cluster radius  $R$  (which would be an exact approximation if all ions were placed on the surface of the cluster), we can estimate how this time scale depends on the characteristic variables of a cluster:

$$\frac{T_0}{V_0} \propto \frac{MR^3}{(N-1)(Z_{\text{final}}/N)^2}. \quad (30)$$

From this equation we can read off how the expansion process changes when the number of atoms  $N$  is changed while keeping all other parameters fixed: if  $V_{\text{atom}} = 4/3\pi r_s^3$  is the volume of one atom inside the cluster, then  $R^3 = N r_s^3$ . Hence, the time scale of the

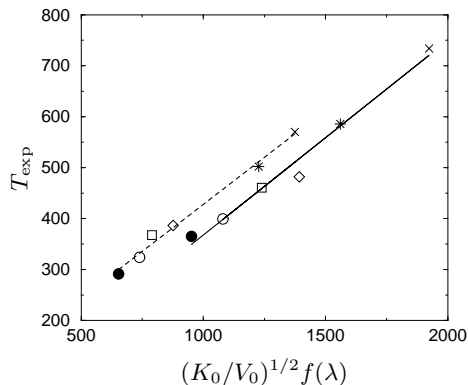


FIG. 20: Expansion time (numerical data) as a function of  $(K_0/V_0)^{1/2} f(\lambda)$  and linear fits (see text). Two different energy normalizations were used:  $F_0 = 0.16$  a.u. (solid line) and  $F_0 = 0.25$  a.u. (dashed line), both at a frequency of  $\omega = 0.055$  a.u. and a pulse length of  $T = 55$  fs. Ar<sub>16</sub>(●), Ar<sub>20</sub>(○), Ar<sub>25</sub>(□), Ar<sub>30</sub>(◇), Kr<sub>16</sub>(★) and Xe<sub>16</sub>(×)

expansion is governed by the factor  $N/(N-1)$ , which depends only weakly on  $N$ . This leads us to the conclusion that indeed the increase of  $T^*$  with  $N$  in Fig. 14 is not due to the expansion process but due to the increase of  $R^*$  with  $N$  only (see Fig. 11).

### A. Scaling of the optimal pulse length

With Eq. (29) at hand we are able to set up a relation between the optimal pulse lengths for various cluster if we make one last assumption: the factor  $\alpha$ , which determines the ratio between the average atomic charge  $\bar{Z}$  driving the expansion up to  $R^*$  and the final charge per atom after the pulse,  $Z_{\text{final}}/N$ , is identical for all clusters. If this hypothesis was true, then  $1-\alpha$  would be a universal measure for the efficiency of the ENIO mechanism.

If  $\alpha$  is the same for all clusters, we get from Eq. (29) a linear relation between the expansion time  $T_{\text{exp}}$  and  $f(\lambda)(T_0/V_0)^{1/2}$ , different for each cluster. This prediction is confirmed by Fig. 20 which shows the expansion times  $T_{\text{exp}} = T^*/2 - T_0$  as a function of the cluster-dependent values of  $(K_0/V_0)^{1/2} f(\lambda)$  for different clusters. We have obtained  $\lambda$  from the respective static calculations for each cluster. A linear fit to the data yields  $\alpha = 0.38$  and  $\alpha = 0.37$  for energy normalized pulses at  $F_0 = 0.16$  and  $F_0 = 0.25$ , respectively. The correlation coefficient is in both cases higher than 0.99. Hence,  $\alpha$  is the same for different clusters, and it is even almost the same for different energy normalizations of the laser

pulse. This result *a posteriori* justifies the approximations we have made in establishing our expansion model.

The fact that  $\alpha$  remains almost the same when changing the pulse normalization is certainly an unexpected result; it is probably valid only for a limited range of pulse energy contents, if one thinks of  $\alpha$  as a measure for the efficiency of ENIO. At least in the limit of a very large pulse energy, when the electric field of the laser is larger than the electric field from the charges in the cluster, we expect the ENIO mechanism to play no important role any more, since the cluster geometry will be washed out. However, the good agreement of the linear fit in Fig. 20 with our numerical data for each of the two normalizations separately points to a deeper scaling relation between the various clusters, the reason for which will be explored in future work.

## VII. SUMMARY AND CONCLUSION

We have developed a quasiclassical model for small rare gas cluster in strong laser fields. This model allows us to investigate the influence of several parameters, like the atomic element and the cluster size, but also the characteristics of the applied laser field. We have shown that, as a function of pulse length, the energy absorption as well as the ionization yield of all but the Ne clusters show a clear maximum when the energy content of the pulse is kept fixed. This behavior has been attributed to the existence of a critical cluster radius  $R^*$ , whose origin could be explained by generalizing the CREI or ENIO concept from diatomic molecules to small rare gas clusters. It was shown that this mechanism is stable against a change of system parameters, even when switching from linear to circular polarization. This is a pronounced difference between clusters and molecules.

Finally, we were able to condense the absorption and expansion process into a simple model and obtained an analytical expression connecting the expansion time and the cluster properties. The validity of this expression has been confirmed by our numerical data.

Future investigations will include the transition to the plasma regime, which we expect to begin at around  $N \approx 10^3$ . In this regime, another critical radius should emerge, when the laser frequency matches the plasma frequency. It will be interesting to see how this additional critical radius evolves with  $N$  and if there is a regime where the  $R^*$  coming from the ENIO process and the plasma related  $R_c^*$  coexist.

We would like the DFG for financial support within the Gerhard Hess-program.

- 
- [1] F. Calvayrac, E. Suraud, and P. Reinhard, J. Phys. B **31**, 1367 (1998).  
 [2] F. Calvayrac, P. Reinhard, E. Suraud, and C. Ullrich,

- Physics Reports **337**, 493 (2000).  
 [3] L. Köller, M. Schumacher, J. Köhn, S. Teuber, J. Tiggesbäumker, and K. Meiwes-Broer, Phys. Rev.

- Lett. **82**, 3783 (1999).
- [4] T. Ditmire, T. Donnelly, A. Rubenchik, R. Falocone, and M. Perry, Phys. Rev. A **53**, 3379 (1996).
- [5] J. Zweiback, T. Ditmire, and M. Perry, Phys. Rev. A **59**, R3166 (1999).
- [6] M. Lezius, S. Dobosz, D. Normand, and M. Schmidt, Phys. Rev. Lett. **80**, 261 (1998).
- [7] J. Purnell, E. Snyder, S. Wei, and A. C. Jr., Chem. Phys. Lett. **229**, 333 (1994).
- [8] E. Springate, N. Hay, J. Tisch, M. Mason, T. Ditmire, M. Hutchinson, and J. Marangos, Phys. Rev. A **61**, 063201 (2000).
- [9] T. Ditmire, J. Tisch, E. Springate, M. Mason, N. Hay, R. Smith, J. Marangos, and M. Hutchinson, Nature **386**, 54 (1997).
- [10] T. Zuo and A. Bandrauk, Phys. Rev. A **52**, R2511 (1995).
- [11] T. Seideman, M. Yvanov, and P. Corkum, Phys. Rev. Lett. **75**, 2819 (1995).
- [12] From this moment on, we neglect the contribution of the Lennard-Jones potential.
- [13] M. Ammosov, N. Delone, and V. Krainov, JETP **64**, 1191 (1986).
- [14] D. Bauer and P. Mulser, Phys. Rev. A **59**, 569 (1999).
- [15] K. Ishikawa and T. Blenski, Phys. Rev. A **62**, 063204 (2000).
- [16] Energy conservation is not automatically guaranteed by just placing the electron at  $r_2$  with no kinetic energy, as one might suspect from Fig. 1. The reason is that the ionic softcore parameter is  $Z$ -dependent and, in addition, differs from the softcore parameter of an electron.
- [17] P. Channell and C. Scovel, Nonlinearity **3**, 231 (1990).
- [18] C. Rose-Petruck, K. Schafer, K. Wilson, and C. Barthly, Phys. Rev. A **55**, 1182 (1997).
- [19] T. Ditmire, Phys. Rev. A **57**, R4094 (1998).
- [20] Landau and Lifshitz, *Quantenmechanik* (Akademie-Verlag Berlin, 1960).
- [21] The cluster radius of course directly corresponds to the mean interionic distance.
- [22] W. Ekardt, PRL **52**, 1925 (1984).
- [23] J. Posthumus, L. Frasiniski, A. Giles, and K. Codling, J. Phys. B **28**, L349 (1995).
- [24] A. Bandrauk and J. Ruel, Phys. Rev. A **59**, 2153 (1999).
- [25] I. Kawata, H. Kono, and A. Bandrauk, PRA **64**, 043411 (2001).
- [26] J. Posthumus, A. Giles, M. Thompson, W. Shaikh, A. Langley, L. Frasiniski, and K. Codling, J. Phys. B **29**, L525 (1996).
- [27] S. Banerjee, G. R. Kumar, and D. Mathur, Phys. Rev. A **60**, R25 (1999).